Journal of Alloys and Compounds 509 (2011) 9675–9678

Contents lists available at ScienceDirect

Journal of Alloys and Compounds

journal homepage: www.elsevier.com/locate/jallcom

Application of dendrite fragmentation to fabricate the homogeneous dispersed structure in undercooled Cu–Co immiscible alloy

W. Yang[a,*], H. Yu[a], J.H. Wang[a], C.C. Cai[a], Z.F. Xu[a], S. Li[b], F. Liu[b], G.C. Yang[b]

[a] National Defence Key Discipline Laboratory of Light Alloy Processing Science and Technology, Nanchang Hangkong University, Nanchang 330063, PR China
[b] State Key Laboratory of Solidification Processing, Northwestern Polytechnical University, Xi'an, Shaanxi 710072, PR China

ARTICLE INFO

Article history:
Received 2 July 2011
Received in revised form 21 July 2011
Accepted 24 July 2011
Available online 29 July 2011

Keywords:
Rapid-solidification
Metals and alloys
Microstructure
Phase transitions

ABSTRACT

The dependence of microstructure on undercooling for $Cu_{50}Co_{50}$ immiscible alloy and the relations between dendrite fragmentation and liquid phase separation were studied by melt-fluxing in combination with cyclic superheating. It is shown that homogeneous dispersed structure can be obtained by dendrite fragmentation because of the increased solute content in primary dendrite, which is advantageous for strengthening dendrite remelting effect and thermal plateau time following recalescence. As for the sample after liquid separation, typical dual-layer structure forms, while dendrite fragmentation still exists and its extent, volume fraction are influenced by the solute contents of two immiscible layers. Quantitative thermodynamic calculation was further performed to support the experimental results.

1. Introduction

Liquid immiscible alloys with a high dispersion and uniform phase distribution structure have excellent mechanical and physical properties and can be used as advanced slide bearings and electrical contact materials [1]. During past decades, a considerable work was performed on synthesizing this ideal structure by fast cooling technique, such as gas atomization and melt spinning, where the motion and coagulation of the separated small liquid droplets can be hindered by the enhanced solidification rate [2–4]. With increasing undercooling by melt fluxing or electromagnetic levitation, rapid solidification can be realized under normal cooling rate as well [5–7]. However, less attention was paid on the formation of uniform and dispersed microstructure by this thermodynamic method, even though it is advantageous for in situ agnostics to understand the physical mechanisms in these rapid transformations [8,9].

Due to the severe rapid heat shock and Rayleigh instability effect during and after recalescence process, dendrite fragmentation occurs universally in the rapid solidification of undercooled melts and the resultant grain-refined microstructure has been detected in many metallic systems, such as Fe–Co [10], Fe–Ni [11], Ni–C [12] and Fe–Ga [13]. With the influence of large mixing enthalpy, Cu–Co alloy presents a metastable liquid miscibility gap. During past decades, many researches were performed on the prediction of liquid separation, separating kinetics, as well as the resultant macroscopic layer structure [14–17]. Nevertheless, a thorough understanding of the dendrite fragmentation phenomenon for undercooled Cu–Co immiscible alloy, especially for its influence and relation with the liquid phase separation process, is still rather limited. Regarding this point, the present work chooses $Cu_{50}Co_{50}$ as the research object and the attention is focused on the dendrite fragmentation regularity before and after liquid separation so as to optimize the fabrication routes for homogeneous dispersed structure.

2. Experimental procedure

The undercooling experiments were performed by melt fluxing in combination with cyclic superheating method. $Cu_{50}Co_{50}$ alloy with a mass of 5 g was in situ melted of copper block and cobalt powder with purity better than 99.98 wt% and 99.8 wt%. The experimental apparatus consists of a high frequency induction heating facility, an infrared pyrometer and a signal recorder. In order to obtain undercooling as large as possible, the superheating–cooling procedure was repeated several times so as to eliminate the heterogeneous catalyst by decomposition, melting, or passivation effect. After the sample had been superheated to the desired temperature for 3–10 min, the induction heater was turned off so that the sample was spontaneously cooled down to room temperature. The heating and cooling curves of the melts were in situ measured by an infrared pyrometer, which were calibrated with a standard PtRh30-/PtRh6 thermocouple and the constant peritectic transformation temperature, i.e., 1385 K determined from the published phase diagram [17]. After experiment, the as-prepared samples were sectioned longitudinally and processed according to standard metallographic procedure. The microstructure morphology, phase structure and element composition were analyzed by using an optical microscope (VHX-600, KEYENCE), X-ray diffraction (XRD, D8X, Cu Kα radiation) and scanning electron microscope (SEM, Quanta 200) equipped with energy dispersive spectroscopy (EDS, INCA).

* Corresponding author. Tel.: +86 791 6453167; fax: +86 791 3953300.
E-mail address: weiyang@mail.nwpu.edu.cn (W. Yang).

0925-8388/$ – see front matter © 2011 Elsevier B.V. All rights reserved.
doi:10.1016/j.jallcom.2011.07.077

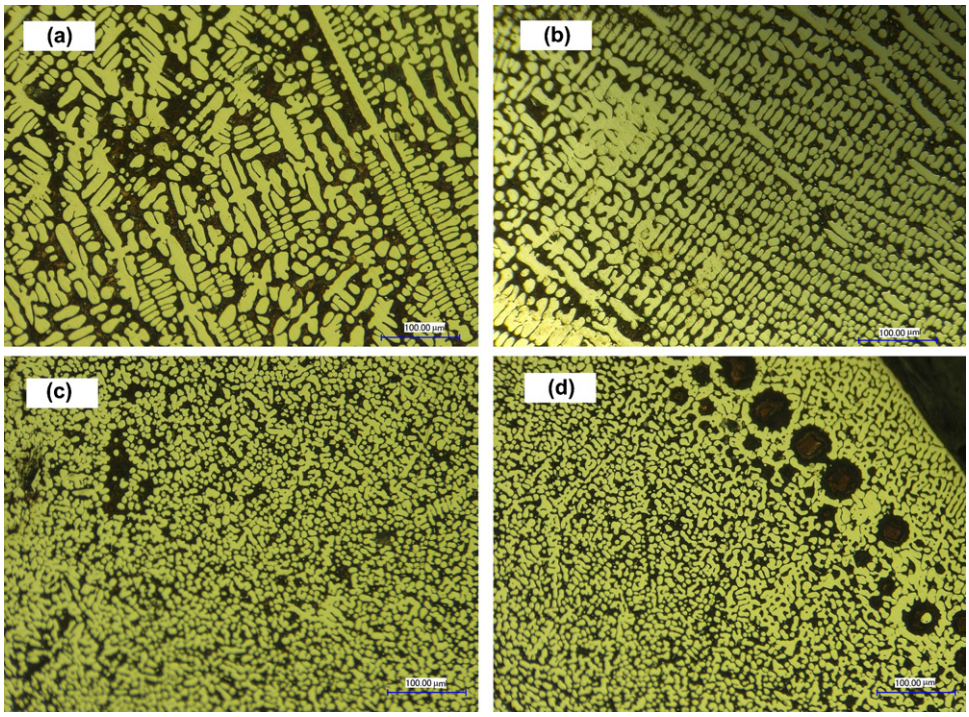

Fig. 1. Microstructure morphologies of $Cu_{50}Co_{50}$ alloy at different undercoolings: (a) $\Delta T = 62$ K; (b) $\Delta T = 105$ K; (c) the center for $\Delta T = 125$ K; (d) the surface for $\Delta T = 125$ K.

3. Results and discussion

3.1. Microstructure morphology as a function of undercooling

Fig. 1 shows the as-solidified microstructure morphologies of $Cu_{50}Co_{50}$ alloy with different undercoolings. If solidification occurs at the undercooling of 62 K, coarse dendrites with well developed primary trunks and secondary arms form primarily (Fig. 1a). After the compositional analysis by EDS, these dendrites were identified as α-Co phase, which is consistent with the reported phase diagram [17]. Obviously, incomplete dendrite fragmentation occurs in this case, which can be indicated by the coexistence of dendrite segments with an average size of ~40 μm and the residual dendrite trunk larger than 200 μm. With increasing undercooling to

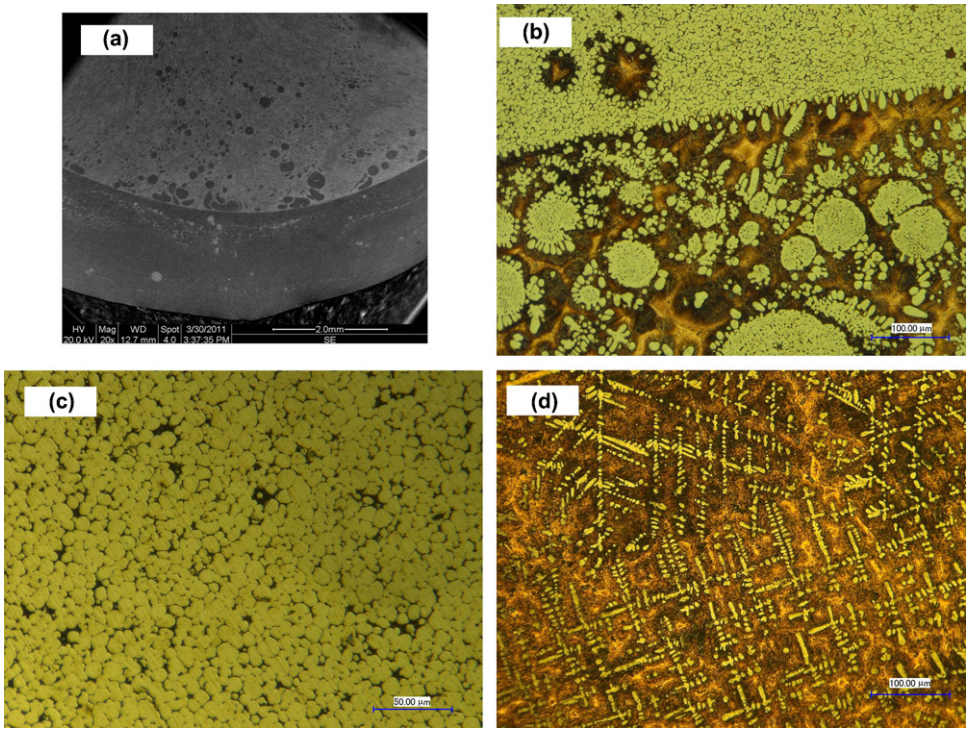

Fig. 2. Microstructure morphologies of $Cu_{50}Co_{50}$ alloy with $\Delta T = 220$ K: (a) SEM–BEI image; (b) the interface region between the Cu-rich and Co-rich layers; (c) dendrite segments in the Co-rich layer and (d) dendrite segments in the Cu-rich layer.

105 K, dendrite fragmentation becomes severer, which generates the reduction of average grain size to ~20 μm (Fig. 1b). Nevertheless, dendrite skeleton can still be observed with the oriented arrangement of fragmented granular grain. As for the undercooling of 125 K, the microstructure contains many finely dispersed Co-rich spheres with diameter less than 10 μm and its distribution is fairly homogeneous (Fig. 1c). According to the as described evolution regulation, its formation can be ascribed to the complete dendrite fragmentation. With increasing distance from the sample center towards the surface, a tendency for phase separation is observed, as inferred by the several Cu-rich regions with round shape due to the minimum of surface energy (Fig. 1d).

With further increasing undercooling, the microstructure differs greatly from the above observed morphologies. Fig. 2a shows the SEM–BEI image for the sample with ΔT = 220 K. It indicates clearly that a typical dual-layer structure takes place due to the occurrence of liquid phase separation and the white and dark areas belong to Cu-rich and Co-rich phases, respectively. The image of the interface between these two layers is given in Fig. 2b, where the collision and coagulation of the dendrites and their small segments (light regions) can be seen clearly. Regarding the fact that larger Co-rich particles are surrounded by the finer droplets in the separated Cu phase and the existence of Cu-rich droplets in the separated Co phase, second liquid separation can be inferred to occur in both layers. Detailed grain morphologies for the Co-rich and Cu-rich layers are shown in Fig. 2c and d, respectively. As for the Co-rich layer, the microstructure is still characterized by the granular grain with the average size of ~5 μm. In comparison with the above undercoolings, the volume fraction of α-Co phase increases significantly. In contrast, Co-rich dendrite skeleton with less volume fraction is observed in the Cu-rich layer due to the slight fragmentation effect (Fig. 2d).

3.2. Phase structure analysis at different undercoolings

To identify the phase structures before and after liquid separation, X-ray diffraction was further employed for the samples with ΔT = 62 K and 220 K, which correspond to mixing and demixing cases separately. As shown in Fig. 3, two fcc phases can be seen due to the coexistence of Cu-rich solid solution (with strong reflection) and Co-rich solid solution (with weak reflection). It is worth noting that the liquid separation process does not affect the component of phase structure, but leads to the reduction of base line levelness for larger undercooling case, which may be caused by the inhomogeneous distribution of different phases after liquid separation, as shown in Fig. 2.

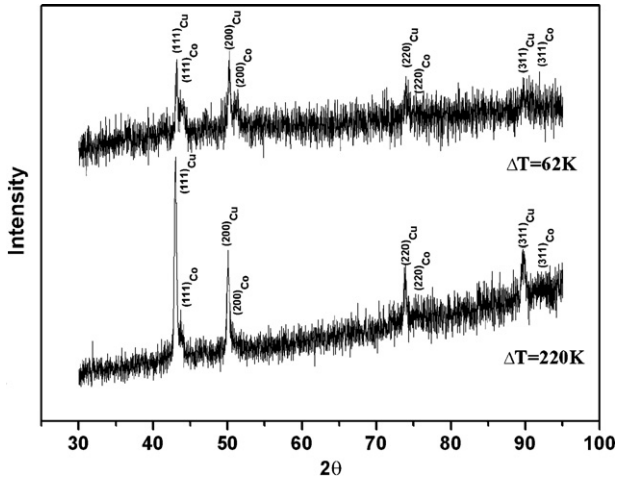

Fig. 3. X-ray diffraction patterns for the samples with ΔT = 62 K and 220 K.

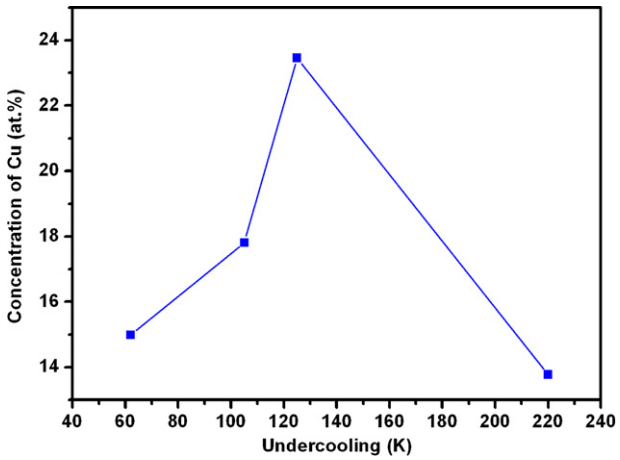

Fig. 4. Concentration of solute Cu in primary α-Co phase as a function of undercooling.

3.3. Analysis of solute concentration in primary phase

Fig. 4 shows the concentrations of solute Cu in primary α-Co phase at different undercoolings, where the result for 220 K is obtained from the Co-rich layer after liquid separation. In principle, there are two possible mechanisms for grain refinement: (1) dendrite break-up [18] or (2) dendrite remelting [19]. The content of solute Cu in α-Co dendrite without liquid separation increases continuously with undercooling due to the enhanced solute trapping effect [20,21]. Consequently, the solidus temperature of primary dendrite is decreased, which will strengthen the dendrite remelting effect during recalescence. With the process of transformation, more and more solute atoms were rejected to residual liquid phase, which increases its content, as well as the range of mushy zone. As a result, the thermal plateau time for dendrite break-up extends. With the combination of these two influences, dendrite fragmentation can be expected more severe and this is consistent with the experimental observation for the sample without liquid separation (Fig. 1). As for the sample of ΔT= 220 K with liquid separation, the concentration of solute Cu in α-Co grain decreases, which can be ascribed to the demixing effect from a thermodynamic equilibrium viewpoint. In such a case, the volume fraction of primary α-Co can be inferred to increase, which is in accord with the as-observed microstructure shown in Fig. 2c.

3.4. Calculation of Gibbs free energy for undercooled liquid

To give a better understanding of the above experimental results, the calculation of Gibbs free energy for liquid is performed with the optimized thermodynamic data by Palumbo et al. [17] and the results are given in Fig. 5. As can be seen clearly, the Gibbs free energy of liquid with the absolute temperature of 1593 K, 1550 K and 1530 K, which corresponds to ΔT = 62 K, 105 K and 125 K with respect to the liquidus temperature 1655 K of $Cu_{50}Co_{50}$ alloy, shows no obvious spinodal feature (Fig. 5a), which is consistent with the above microstructure observation with no apparent liquid separation (Fig. 1a–c). Strictly speaking, slight spinodal is actually existed for 1550 K and 1530 K. This discrepancy can be ascribed to the uncertainty of temperature measurement. In addition, it agrees well with the above observed tendency of liquid separation at the surface area for the sample with ΔT = 125 K (Fig. 1d). As for T = 1435 K, the Gibbs free energy curve shows a typical spinodal shape with the common tangent points of 0.168 and 0.862

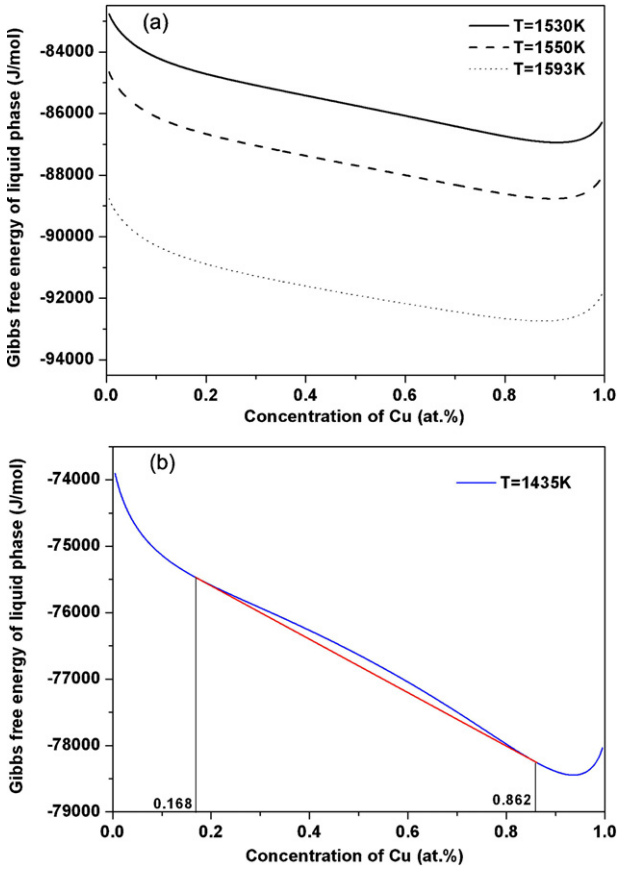

Fig. 5. Gibbs free energy curves of liquid phase for Cu–Co alloy at different temperatures.

(Fig. 5b) of element Cu, which indicates the occurrence of liquid separation and agrees once again with the observed experimental results (Fig. 2). The concentration of solute Cu in Co-rich phase is 16.8 at.%, this can also be used to explain the decrease of its content shown in Fig. 4. Moreover, the demixing phenomenon in Cu and Co components also induces the volume fraction variation in the separated two layers.

4. Conclusions

Dendrite fragmentation and its association with liquid phase separation were investigated in undercooled $Cu_{50}Co_{50}$ immiscible alloy by adopting melt-fluxing and cyclic superheating. As for the undercooling of 62 K and 105 K, alloys solidifying from the homogeneous liquid possess a normal dendritic skeleton with the gradual reduction of dendrite segments. With increasing undercooling to 125 K, finely dispersed Co-rich spheres with diameters less than 10 μm were obtained due to the complete dendrite fragmentation. In contrast, liquid phase separation at $\Delta T = 220$ K brought a typical dual-layer structure, while dendrite fragmentation effect still exist and its content, as well as volume fraction are influenced by the solute contents of two separated layers. The experimental results were further supported by the quantitative thermodynamic calculation, which is useful for the fabrication of homogeneous dispersed structure for immiscible alloy.

Acknowledgements

The work is supported by the fund of the State Key Laboratory of Solidification Processing in NWPU (SKLSP201118), Scientific Starting Foundation for Doctorate Research in Nanchang Hangkong University (EA201003234), the Natural Science Foundation of China (Grant nos. 50771084; 51071127) and the National Basic Research Program of China (973Program, 2011CB610403). W. Yang is also grateful to Prof. M. Palumbo and Dr. Z.P. Sun for the help of thermodynamic calculation.

References

[1] E. Ma, Prog. Mater. Sci. 50 (2005) 413–509.
[2] J. He, H.Q. Li, B.J. Yang, J.Z. Zhao, H.F. Zhang, Z.Q. Hu, J. Alloys Compd. 489 (2010) 535–540.
[3] J.J. Guo, Y. Liu, J. Jia, Y.Q. Su, J.Z. Zhao, Scripta Mater. 45 (2001) 1197–1204.
[4] T.J. Rathz, M.B. Robinson, D. Li, J. Mater. Sci. 36 (2001) 1183–1188.
[5] H.X. Zheng, M.X. Xia, J. Liu, J.G. Li, J. Alloys Compd. 388 (2005) 172–176.
[6] N. Liu, G.C. Yang, W. Yang, Physica B 406 (2011) 957–962.
[7] M.J. Li, K. Nagashio, K. Kuribayashi, Scripta Mater. 47 (2002) 213–218.
[8] D.M. Herlach, Mater. Sci. Eng. R 12 (1994) 177–272.
[9] F. Liu, G.C. Yang, Int. Mater. Rev. 51 (2006) 145–170.
[10] N. Liu, F. Liu, G.C. Yang, Y.Z. Chen, C.L. Yang, Y.H. Zhou, J. Alloys Compd. 455 (2008) L6–L9.
[11] Y.Z. Chen, G.C. Yang, F. Liu, J. Cryst. Growth 282 (2005) 490–497.
[12] K. Eckler, A.F. Norman, F. Gätner, J. Cryst. Growth 173 (1997) 528–540.
[13] J.K. Zhou, J.G. Li, J. Alloys Compd. 461 (2007) 113–116.
[14] W. Sha, X. Wu, K.G. Keong, Electroless Copper and Nickel-Phosphorus Plating: Processing Characterisation and Modelling, first ed., Woodhead Publishing Limited, Cambridge, 2010.
[15] C.D. Cao, D.M. Herlach, M. Kolbe, Scripta Mater. 48 (2003) 5–9.
[16] Y. Yu, X.J. Liu, C.P. Wang, Z.P. Jiang, J. Mater. Res. 25 (2010) 1706–1717.
[17] M. Palumbo, S. Curiotto, L. Battezzati, Calphad 30 (2006) 171–178.
[18] Karma, J. Non-Equilibr. Proc. 11 (1998) 201–232.
[19] J.F. Li, Y.H. Zhou, G.C. Yang, Mater. Sci. Eng. A 277 (2000) 161–168.
[20] M.J. Aziz, Phys. Rev. Lett. 56 (1986) 2489–2493.
[21] W. Yang, F. Liu, H.F. Wang, G.C. Yang, Y.H. Zhou, J. Alloys Compd. 470 (2009) L13–L16.